molecular pharmaceutics

Article

Cite This: Mol. Pharmaceutics 2018, 15, 1534−1547

Computational Modeling of Antiviral Drug Diffusion from Poly(lactic-*co*-glycolic-acid) Fibers and Multicompartment Pharmacokinetics for Application to the Female Reproductive Tract

Michael E. Halwes,[†] Kevin M. Tyo,[‡,⊥] Jill M. Steinbach-Rankins,[†,‡,§,⊥,∥] and Hermann B. Frieboes*[,†,‡,¶,∥]

[†]Department of Bioengineering, University of Louisville, Louisville, Kentucky 40292, United States

[‡]Department of Pharmacology and Toxicology, [§]Department of Microbiology and Immunology, [⊥]Center for Predictive Medicine, and [¶]James Graham Brown Cancer Center, University of Louisville, Louisville, Kentucky 40292, United States

ABSTRACT: The need for more versatile technologies to deliver antiviral agents to the female reproductive tract (FRT) has spurred the development of on-demand and sustained-release platforms. Electrospun fibers (EFs), in particular, have recently been applied to FRT delivery, resulting in an alternative dosage form with the potential to provide protection and therapeutic effect against a variety of infection types. However, a multitude of fabrication parameters, as well as the resulting complexities of solvent−drug, drug−polymer, and solvent−polymer interactions, are known to significantly impact the loading and release of incorporated agents. Numerous processing parameters, in addition to their combined interactions, can hinder the iterative development of fiber formulations to achieve optimal release for particular durations, doses, and polymer−drug types. The experimental effort to design and develop EFs could benefit from mathematical analysis and computational simulation that predictively evaluate combinations of parameters to meet product design needs. Here, existing modeling efforts are leveraged to develop a simulation platform that correlates and predicts the delivery of relevant small molecule antivirals from EFs that have been recently applied to target sexually transmitted infections (STIs). A pair of mathematical models is coupled to simulate the release of two structurally similar small molecule antiretroviral reverse transcriptase inhibitors, Tenofovir (TFV) and Tenofovir disoproxil fumarate (TDF), from poly(lactic-*co*-glycolic acid) (PLGA) EFs, and to evaluate how changes in the system parameters affect the distribution of encapsulated agent in a three-compartment model of the vaginal epithelium. The results indicate that factors such as fiber diameter, mesh thickness, antiviral diffusivity, and fiber geometry can be simulated to create an accurate model that distinguishes the different release patterns of TFV and TDF from EFs, and that enables detailed evaluation of the associated pharmacokinetics. This simulation platform offers a basis with which to further study EF parameters and their effect on antiviral release and pharmacokinetics in the FRT.

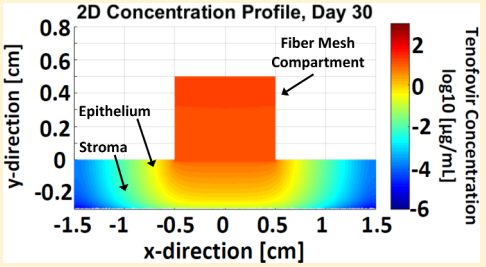

KEYWORDS: *PLGA, electrospun fibers, mathematical modeling, computational simulation, pharmacokinetics, antiretroviral drug, human immunodeficiency virus (HIV), Tenofovir (TFV), Tenofovir disoproxil fumarate (TDF), sexually transmitted infections (STI)*

1. INTRODUCTION

Electrospun fibers (EFs) have emerged as a new delivery vehicle alternative to provide high encapsulation and the tunable release of antiviral agents to the female reproductive tract (FRT).[1−3] However, as next-generation alternative and multipurpose delivery vehicles are developed for localized intravaginal applications, the complexity of encapsulants, materials, fabrication parameters, and combinations thereof will make it more difficult to iteratively design EFs with "optimal" release characteristics and to predict the distribution of these agents in the FRT. Moreover, the development and utilization of EFs for intravaginal application is in the nascent stages, with few studies of active agent distribution from fibers into the (murine) reproductive tract conducted to date.[4−6] Even with gradual progress, the scale-up for clinical applications will require the ability to more easily assess the impact that small (or large) molecule size, and other physical and chemical alterations of active agents with a given delivery platform, have in achieving tissue distribution and penetration. Recently a study highlighted the release differences of the small molecule active agent Tenofovir disoproxil fumarate (TDF), relative to Tenofovir (TFV), from electrospun fibers, noting that even minute alterations in chemical structure can impart significant differences in release profiles.[7] The results emphasized the somewhat counterintuitive impact that small alterations in active agent selection and fiber composition can have in obtaining desired release characteristics.

To help address these considerations, mathematical modeling has been applied to analyze the release and transport of active agents from electrospun fibers.[8−10] These models could be made applicable to a variety of vehicles, such as

Received: December 4, 2017
Revised: February 17, 2018
Accepted: February 21, 2018
Published: February 26, 2018

DOI: 10.1021/acs.molpharmaceut.7b01089
Mol. Pharmaceutics 2018, 15, 1534−1547

nanoparticles and liposomes, as well as a diversity of materials, including natural polymers, synthetic polymers, and lipids. In addition to these vehicle-specific models, pharmacokinetic models have been created to analyze the diffusion of molecular species through fluids and tissues.[11−13] Particularly for early developing technologies, the utilization of mathematical models is highly desirable to elucidate delivery parameters and understand their application in new physiological environments or dosage forms. More specifically, mathematical modeling has the potential to benefit research that utilizes existing carriers with known *in vitro* release profiles. In these cases, a greater depth of information may be gained and translated to material alterations to improve clinical translation.

One of the primary goals in considering different polymer types, active agents, and fabrication conditions in the design of EFs for intravaginal applications is to develop efficacious fibers that release agents in an inducible or prolonged manner. In recent work, we have evaluated polymeric nanoparticle and electrospun fiber delivery platforms to establish protection and treatment against herpes simplex virus type 2 (HSV-2) and human immunodeficiency virus (HIV) infection in the FRT.[1,14,15] Biocompatible polymers such as poly(lactic-*co*-glycolic-acid) (PLGA) are frequently employed for the synthesis of electrospun fibers and nanoparticles due to their biocompatibility and tunable release properties. Previous experiments[7,14,16] have elucidated the response of these drug delivery vehicles to varying parameters, including relative concentrations of lactic and glycolic acid, tendencies of varying geometries to degrade via bulk versus surface degradation, and the effect of encapsulated or surface-conjugated agents on polymer scaffold release and degradation. A focus of our and others' work has been to utilize a given polymeric platform to deliver different molecules of choice (e.g., small molecule antivirals, proteins, genes). A primary challenge has been predicting and understanding the differing release profiles that result based on small modifications to molecules, which can have a significant impact on duration of use and efficacy. An impactful example noted above is that seemingly minor alterations of small molecule antivirals, such as TFV to TDF, have been shown to significantly affect release profiles from the same polymer vehicle under similar environmental conditions[7,16]

The goal of this study is to develop and validate a modeling framework that predicts the release of small molecule antiviral drugs, such as TFV and TDF, from uniaxial PLGA fibers. We hypothesize that the development of a system that can predict the somewhat large distribution differences resulting from very small structural differences would provide a foundation for future studies to predict the release and transport of active agents in the FRT. A longer-tem goal is to provide insight into the trade-offs between specific physical and chemical compositions of active agents, in combination with different polymer types and fabrication parameters, to relate to release profiles *in vitro* and *in vivo*.

Toward these efforts, previous investigations into the sustained-release and degradative properties of polymer scaffolds have relied largely on lumped parameter models. However, with the increased applicability of finite element methods, polymer degradation can be more rigorously simulated. Casalini et al.[17] recently presented a model to study the degradation of PLGA polymer chains, specifically in nanoparticle systems. In parallel, Katz and co-workers have pioneered multicompartmental models to investigate the pharmacokinetic (PK) diffusion of TFV from microbicide gels in the vaginal environment.[11,12] We build upon this previous modeling and experimental work to simulate electrospun PLGA fiber degradation and release of TFV and TDF, and the resulting drug spatiotemporal distribution in vaginal tissue. These structurally similar small molecule drugs are commonly used in investigative microbicides to prevent HIV and HSV-2 infection. The underlying mathematics of the model in ref 17 was converted from spherical to cylindrical coordinates to simulate degradation and release from an electrospun PLGA fiber. The model output was then incorporated into a 2D multicompartmental diffusion model building upon ref 11 to simulate the release of TFV from a fibrous mesh into the vaginal epithelium and stroma. The resulting framework consisting of two coupled models provides the capability to study variation in fiber degradation and drug release, and how these parameters in turn may affect the tissue distribution, without recourse to excessive experimentation. The model parameters were matched with either TFV data previously presented in the literature[11,12,16] or with our experimental data obtained *in vitro* with a novel TDF-containing PLGA electrospun fiber vehicle designed for localized intravaginal delivery.[18] To account for possible anisotropies of epithelial tissues in the context of diffusivity, we further assessed the distribution of drug concentration in both the transverse and lateral tissue directions to determine if clinically relevant concentrations could be established and maintained during therapeutic application. This modeling framework enables the evaluation of key parameters related to drug-loaded PLGA fibers, including fiber degradation and drug molecule release, and the resulting diffusion of drug in a multicompartmental representation of the FRT.

2. METHODS

2.1. System Geometry. The system represents a sample of an electrospun fiber mesh placed in fluid over a layer of vaginal tissue. The fluid domain is modeled as a cylinder with a 0.5 cm radius (r_F) and 0.5 cm thickness (h_F), resulting in a volume, V_{mesh}, of 0.393 cm^3 (Figure 1). The fiber microstructures are

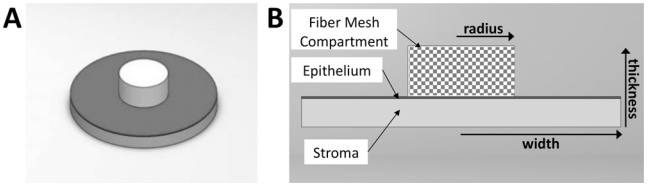

Figure 1. System geometry to model tenofovir (TFV) and tenofovir disproxil fumarate (TDF) release from PLGA fibers. The model simulates a single long fiber that represents the cumulative length of every fiber in a mesh of the given dimensions. (A) Isometric view of the system geometry; (B) system cross-section. The compartment representing the fiber mesh is 0.5 cm thick and has a radius of 0.5 cm. The widths of the epithelial and stromal compartments are both 3 cm, while the thicknesses of the epithelium and stroma are 0.02 and 0.28 cm, respectively. Both diagrams are shown to scale.

modeled as uniform cylinders with a diameter of 1 μm (r_f = 0.5 μm). The same fiber geometry was used for the same percentage loading of TFV and TDF. The vaginal tissue consists of two layers: a 200 μm thick (h_E) epithelial region and a 2.8 mm thick (h_S) stromal region. Both layers of the vaginal tissue in this model have a diameter of 3 cm (r_C), with the fiber

DOI: 10.1021/acs.molpharmaceut.7b01089
Mol. Pharmaceutics 2018, 15, 1534−1547

mesh placed centrally, to provide the drug molecules adequate distance for lateral diffusion. The selected thickness corresponds to an epithelial layer of approximately 15−20 cells. The total volume of the tissue, V_C, is calculated to be 2.121 cm^3.

2.2. Drug Release from Polymer Fiber. *2.2.1. Model Formulation.* The first component of the system represents the release of encapsulated drug from individual fibers as the surrounding polymer matrix degrades in an aqueous environment. Mathematical equations governing these processes in a PLGA microparticle-based system have been discussed previously[17] and are adapted here to a cylindrical coordinate system for the fiber representation.

The system geometry consists only of the interior of one representative fiber. Since the drug is assumed to be homogeneously distributed throughout the fiber prior to the beginning of the *in silico* experiment, diffusion of all species occurs only in the radial direction, and therefore, symmetry is assumed at the fiber center. Initially, individual equations governing the degradation of polymer chains were created for each polymer chain length. However, since PLGA can form polymer chains of upward of 10 000 repeating units, this strategy is not computationally feasible, and the method of statistical moments was instead applied to all polymer chains of chain length $n > 9$. The generic kth order statistical moment is defined as

$$\mu_k = \sum_{n=1}^{\infty} ((n)^k C_n) \tag{1}$$

where n is the chain length (or degree of polymerization), and C_n is the concentration of polymer chains of said chain length. In this context, the statistical moments represent physical characteristics of the system. The concentration of polymer per unit volume is represented by μ_0, while μ_1 is the concentration of monomers per unit volume, and μ_2 is a measure of polymer polydispersity. Using the first, second, and third order statistical moments, the differential equations governing the temporal change in polymer chain concentration at any point within the cylindrical fiber can be described as follows:

$$\frac{\partial C_M}{\partial t} = \frac{1}{r}\frac{\partial}{\partial r}\left(D_M r \frac{\partial C_M}{\partial r}\right) + 2k_d C_w(\mu_0 - C_M)\mu_0 \tag{2a}$$

$$\frac{\partial C_n}{\partial t} = \frac{1}{r}\frac{\partial}{\partial r}\left(D_n r \frac{\partial C_n}{\partial r}\right) + 2k_d C_w\left(\mu_0 - \sum_{j=1}^{n} C_j\right)\mu_0 - (n-1)k_d C_w C_n \mu_0 \quad 2 \le n \le 9 \tag{2b}$$

C_M, C_n, and C_W are the concentrations of polymer monomers, polymer oligomers of chain length 2 to 9, and water, respectively, and r is the radius of the cylinder. D_M and D_n are the diffusion coefficients of the respective species in water, and k_d is a kinetic rate constant for the degradation process. PLGA has been previously classified as a bulk (rather than surface) erosion polymer,[19] and therefore, the diffusion of water into the polymer matrix can be modeled as follows:

$$\frac{\partial C_W}{\partial t} = \frac{1}{r}\frac{\partial}{\partial r}\left(D_W r \frac{\partial C_W}{\partial r}\right) - k_d C_w(\mu_1 - \mu_0)\mu_0 \tag{3}$$

Partial differential equations governing the diffusion and degradation of polymers of length greater than 9 can be formulated using the statistical moments:

$$\frac{\partial \mu_0}{\partial t} = \sum_{j=1}^{9} \frac{1}{r}\frac{\partial}{\partial r}\left(D_j r \frac{\partial C_j}{\partial r}\right) + k_d C_w(\mu_1 - \mu_0)\mu_0 \tag{4a}$$

$$\frac{\partial \mu_1}{\partial t} = \sum_{j=1}^{9} \frac{j}{r}\frac{\partial}{\partial r}\left(D_j r \frac{\partial C_j}{\partial r}\right) \tag{4b}$$

$$\frac{\partial \mu_2}{\partial t} = \sum_{j=1}^{9} \frac{j^2}{r}\frac{\partial}{\partial r}\left(D_j r \frac{\partial C_j}{\partial r}\right) + \frac{k_d C_w \mu_0}{3}\left(\mu_1 - 2\frac{{\mu_2}^2}{\mu_1} + \frac{\mu_2 \mu_1}{\mu_0}\right) \tag{4c}$$

Collectively, eqs 2, 3, and 4 represent 13 equations that were evaluated at each spatial point in the system. In addition to polymer degradation and diffusion, the system modeled diffusion of drug molecules that had been encapsulated in the polymer matrix. While in a physical system there is an additional process where drug crystals encapsulated in the polymer matrix solubilize prior to diffusion, previous investigations[17] have found that additional equations modeling this behavior do not contribute meaningful differences to the model results.

The change in drug concentration C_D is

$$\frac{\partial C_D}{\partial t} = \frac{1}{r}\frac{\partial}{\partial r}\left(D_{D,eff} r \frac{\partial C_D}{\partial r}\right) \tag{5}$$

where $D_{D,eff}$ is the effective diffusion coefficient of drug through the polymer matrix. This introduces an important aspect of this particular system of equations: as the polymer chains inside the fiber continue to degrade, all of the respective diffusing species experience a decrease in hindrance by the polymer chains and consequently an increase in diffusivity, represented by a changing diffusion coefficient as the simulation proceeds. This is described by

$$D_{i,eff} = {D_{i,eff}}^0 \exp\left[2.5\left(1 - \frac{MW_n(t, r)}{MW_n(t=0)}\right)^{0.5}\right] \tag{6}$$

where $D_{I,eff}$ is the effective diffusion coefficient for each of the species (monomers, oligomers, water, and drug), while ${D_{i,eff}}^0$ is the initial diffusion coefficient for each of the species. MW_n is the number-averaged molecular weight, which can be calculated using the already-defined statistical moments:

$$MW_n = \frac{\mu_1}{\mu_0} MW_{mon} \tag{7}$$

where MW_{mon} is the monomer molecular weight.

Variation in TFV and TDF kinetics was achieved by changing the effective diffusion coefficient of the drug molecule in the polymer matrix. This value was 1×10^{-17} cm^2/s for TFV and 3×10^{-15} cm^2/s for TDF. We note that TFV and TDF differ not only in their molecular weight but also in their water solubility. TFV has a water solubility of ~2 mg/mL, while TDF is six-times more water-soluble (>13.4 mg/mL). Accordingly, diffusion in the polymer matrix is expected to reflect these differences.

2.2.2. Boundary Conditions. Since the model was evaluated using cylindrical coordinates, the two boundaries to consider are the center of the fiber ($r = 0$) and the edge of the fiber ($r = R$). Symmetry was assumed at the center of the fiber; therefore,

DOI: 10.1021/acs.molpharmaceut.7b01089
Mol. Pharmaceutics 2018, 15, 1534−1547

$$\left.\frac{\partial C_i}{\partial r}\right|_{r=0} = 0 \tag{8a}$$

$$\left.\frac{\partial D_i}{\partial r}\right|_{r=0} = 0 \tag{8b}$$

where C_i is the concentration of a particular species (monomer, oligomer, drug, and water) and D_i is the associated diffusion coefficient.

At the fiber edge, there is a mass transfer of drug molecules, monomers, oligomers, and water to the outside aqueous environment:

$$-D_i(r=R)\left.\frac{\partial C_i}{\partial t}\right|_{r=R} = k_{C,i}^{ext}(C_{b,i} - C_i(r=R)) \tag{9}$$

where $C_{b,i}$ is the concentration of each respective species in the surrounding environment. This was assumed to be 0 for monomer, oligomer, and drug and 0.055 mol cm^{-3} for water.[17] The assumption of null concentration for the diffusive species is based on the assumption that in physiological systems the turnover of the surrounding fluid would constitute a sink condition. This enables model validation with controlled release experiments *in vitro*. The mass transfer coefficient for each species is $k_{C,i}^{ext}$, estimated using the Sherwood number for the system, a dimensionless number used in mass transfer operations to evaluate the ratio of convective mass transfer and diffusive mass transport.[20] For a system with fluid flow over a cylinder, the Sherwood number is calculated as follows:

$$Sh = 2 = \frac{2k_{C,i}^{ext}R}{D_{i,w}} \tag{10}$$

where R is the radius of the cylinder and $D_{i,w}$ is the diffusion coefficient of the respective species.

2.2.3. Initial Conditions. At time $t = 0$, null conditions are assumed for water, monomer, and oligomers, since the fibers are assumed to be anhydrous and devoid of short chains. The initial concentration of drug, $C_{D,0}$ was taken to be 15% w/w for the PLGA nanofibers, as had been used in the experimental data used to validate the model.[7,16] This corresponded to 0.9392 g of TFV loaded into the fibers. Initial conditions for the statistical moments are calculated as follows:

$$\mu_0(t=0) = \frac{\rho_{pol}}{MW_n(t=0)} \tag{11a}$$

$$\mu_1(t=0) = \frac{MW_n(t=0)}{MW_{mon}}\mu_0(t=0) \tag{11b}$$

$$\mu_2(t=0) = \frac{\mu_1^{\,2}(t=0)}{\mu_0(t=0)}PD(t=0) \tag{11c}$$

where ρ_{pol} is the polymer density and PD is the polydispersity of the fiber mesh.

2.2.4. Use of Method of Lines. The systems presented contain complex partial differential equations that lack an analytical solution. To simplify the system of equations and obtain a numerical solution, the method of lines was employed to effectively remove the radial direction from the system. In lieu of having the radial direction, an array was created with indices corresponding to radial positions within the fiber. The radial direction was discretized into 400 spatial points, sufficient to ensure system stability. While presenting each of the given equations in their revised form would be overly exhaustive, the method of lines approximations for first and second derivatives are presented below to aid in developing the Laplacian terms in the diffusion equations and the boundary conditions:

$$\frac{\partial C}{\partial r} = \frac{C(i+1) - C(i-1)}{2\Delta r} \tag{12a}$$

$$\frac{\partial^2 C}{\partial r^2} = \frac{C(i+1) - 2\times C(i) + C(i-1)}{\Delta r^2} \tag{12b}$$

By using eq 12, all previous equations and boundary conditions can be reformulated to remove the radial direction.

2.2.5. Use of MATLAB To Obtain the Numerical Solution. The MATLAB ode15s solver was used to solve the system of equations. At each spatial point, there were 14 equations to be evaluated. These equations were inserted into an array defining the rate of change in the solution variables (concentrations, statistical moments, etc.) with a length equal to 14-times the number of spatial points. To achieve system stability, the number of spatial points and duration of the solution could be adjusted. Each time this function containing the array of equations was called by the solver, the localized changes in number-averaged MW were calculated and subsequently used to reevaluate the D_{eff} for water, oligomers, and drug for the particular time point.

To increase the computational efficiency of the model, the MATLAB JPattern option was supplied to the ode15s solver.[21] The JPattern defines the overall structure of the Jacobian, the matrix defining the relationships between the derivate terms and system variables. The JPattern's structure for a system with a number of derivative terms:

$$\frac{\partial C_1}{\partial t}, \frac{\partial C_2}{\partial t}, \ldots \frac{\partial C_{i-1}}{\partial t}, \frac{\partial C_i}{\partial t}$$

would be as follows:

$$\begin{array}{c} C_1 \quad C_2 \quad \cdots \\ \begin{matrix} \frac{\partial C_1}{\partial t} \\ \frac{\partial C_2}{\partial t} \\ \vdots \end{matrix} \begin{bmatrix} 1 & 1 & 0 \\ 1 & 1 & \ldots \\ 0 & \vdots & \ddots \end{bmatrix} \end{array}$$

where each matrix entry is either a zero or nonzero value. A nonzero value indicates that the differential term corresponding to that row is somehow dependent on the solution variable corresponding to that column, without giving any specific information on how the two are related. When the JPattern is not supplied to the ode15s solver, MATLAB attempts to evaluate the Jacobian at each entry, resulting in a system that is prohibitively computationally expensive. Given the nature of Method of Lines applications, the Jacobian is a sparse matrix that follows a generally tridiagonal form, therefore an indexing pattern can be used to create the JPattern.

The system was solved, and the concentration of drug in the particle was plotted over time, to evaluate cumulative release of drug from a fiber mesh sample. Instead of modeling multiple fibers in close proximity to one another, as would be observed with a real fiber mesh sample, the model evaluated the drug released from one fiber of length equal to that of the cumulative

DOI: 10.1021/acs.molpharmaceut.7b01089
Mol. Pharmaceutics 2018, 15, 1534−1547

Table 1. Design Parameters: System Geometry, Degradation Model, and Multicompartmental Model

parameter	meaning	value	source
R_F	Diameter of individual fiber	1.0, 2.0, 4.0 μm	Literature[16]
H_F	Thickness of fiber sample	0.5 cm	Estimated
V_F	Fiber mesh volume	0.393 cm^3	Calculated as the volume of a cylinder based on radius and thickness of the fiber compartment.
R_E	Diameter of epithelium	3.0 cm	Estimated
H_E	Thickness of epithelium	0.02 cm	Literature[11]
R_S	Diameter of stroma	3.0 cm	Estimated
H_S	Thickness of stroma	0.28 cm	Literature[11]
V_C	Volume of tissue	2.121 cm^3	Cylindrical volume derived from radii and thicknesses of the epithelium and stroma compartments
$D_{D,eff}$	Diffusion coefficient in polymer matrix		Estimated
	For TFV:	1×10^{-17} cm^2/s	
	For TDF:	3×10^{-15} cm^2/s	
D_W	Diffusion coefficient, water in polymer matrix	1×10^{-8} cm^2/s	Literature[17]
D_O	Diffusion coefficient, oligomer in polymer matrix	1×10^{-10} cm^2/s	Literature[17]
$D_{D,w}$	Diffusion coefficient, TFV in water	6.7×10^{-6} cm^2/s	Calculated from Stokes−Einstein equation and estimation of radius (www.molinspiration.com)
$D_{O,W}$	Diffusion coefficient, oligomer in water	1×10^{-6} cm^2/s	Literature[17]
$D_{W,W}$	Diffusion coefficient, water in water	1×10^{-5} cm^2/s	Literature[17]
D_F	Diffusion coefficient, TFV in fluid compartment	6×10^{-6} cm^2/s	Literature[11,12]
D_E	Diffusion coefficient, TFV in epithelium	7×10^{-8} cm^2/s	Literature[12]
D_S	Diffusion coefficient, TFV in stroma	4×10^{-7} cm^2/s	Literature[12]
K_d	Degradation rate constant	0.1 cm^6/mol^2	Matched to empirical data[16]
K_D	Loss rate constant, due to vaginal fluid turnover	1.22 h^{-1}	Literature[12]
K_L	Loss rate constant, due to drug leaking into stromal vasculature	0.122 h^{-1}	Literature[11]
ρ_{pol}	Polymer density	1.34 g/cm^3	Literature[9]
$K_{c,i}^{ext}$	Mass transfer coefficient	From Sherwood number	Derived from system geometry
$C_{b,i}$	Bulk phase concentration	0 for all except 0.055 mol/cm^3 for water	Literature[17]
$C_{D,0}$	Initial drug concentration	15% w/w relative to polymer mass, 0.9392g TFV	Literature[16]
$C_{w,0}$	Initial water concentration in fiber	0	Literature[17]
$C_{N,0}$	Initial monomer/oligomer concentration in fiber	0	Literature[17]
numPoints	Number of spatial points	400	Estimated
t	Time (duration)	30 days	Estimated

length of fibers in a fiber mesh. This length was dependent upon the density of the fiber, the overall dimensions of the fiber mesh sample, and the porosity of the fiber mesh sample.

2.2.6. Model Validation. To prove the logical validity of the degradation model, a separate run of the model was executed, this time with the mass transfer boundary condition at the outer model boundary removed. The lack of drug loss from the system under these conditions proved that drug concentration was not being lost due to any unforeseen computation or model error.

2.3. Multicompartmental Diffusion Model. A second model, inspired by ref 11, was created to simulate the diffusion of drug from the fiber mesh sample into the vaginal epithelium and stroma. To accomplish this, the MATLAB Partial Differential Equation Toolbox was used to create a 2D multicompartmental system of differential equations (Mathworks. MATLAB. 7.11.0 ed. MathWorks Inc.: Natick, MA; 2010).

2.3.1. System Geometry. The system domain consisted of three 2D compartments, aligned along their center axes, correlating with a cross-section of the aforementioned geometry: a 0.75 cm × 0.5 cm (w_F x h_F) rectangle for the fiber sample, a 3 cm × 0.02 cm rectangle for the vaginal epithelium, and a 3 cm × 0.28 cm rectangle for the vaginal stroma. The system was solved over the same amount of time as the previous model, 30 days.

Previous studies have investigated the one-dimensional diffusion of TFV and other drug molecules through vaginal tissue.[11−13] Here, a two-dimensional model is presented to investigate the effects that the possible anisotropy of vaginal tissue could have on drug molecule diffusion. Since the cells of the lower vaginal epithelium exhibit squamous stratified morphology, it was hypothesized that drug molecules might more readily diffuse laterally along the interstitial space than transversely through the cell layers. To model this, the diffusion coefficients were defined as 2 × 2 matrices:

$$D = \begin{bmatrix} D_x & 0 \\ 0 & D_y \end{bmatrix}$$

where D_X is the lateral diffusion coefficient and D_Y is the transverse diffusion coefficient.

DOI: 10.1021/acs.molpharmaceut.7b01089
Mol. Pharmaceutics 2018, 15, 1534−1547

2.3.2. Governing Equations. Simple second-order diffusion was used to describe the movement of drug molecules through the various compartments. Concentration loss terms were included in the equations for the fiber and stroma regions, due respectively to clearance via vaginal fluid turnover and drug molecules leaking into blood vessels in the stroma:

$$\frac{\partial C}{\partial t} = \nabla\cdot(D_F\nabla C) - k_D C + f \tag{13a}$$

$$\frac{\partial C}{\partial t} = \nabla\cdot(D_E\nabla C) \tag{13b}$$

$$\frac{\partial C}{\partial t} = \nabla\cdot(D_S\nabla C) - k_L C \tag{13c}$$

where D_F, D_E, and D_S represent the drug diffusivity in the fiber mesh, epithelium, and stroma, respectively. The k_D and k_L terms are the rate constants for loss due to dilution (clearance by vaginal fluid turnover) and leakage. The f term represents how the data from the degradation model was incorporated into the multicompartmental model. The f term is a forcing function that is equal to the cumulative sum of the amount of drug concentration that has come out of the fiber in the degradation model. When the degradation model was solved, an array was created defining the loss of concentration from the system at each of the time points supplied to the ode15s solver. This array was used in creating a nonconstant coefficient for the MATLAB solver during the solving of the multicompartmental model. For time points between those contained explicitly in the source array, linear interpolation was used to estimate the source term. Even though the equations governing the release of drug from the fiber in the degradation model are not linear, the high sample rate of the source array gives linear interpolation results sufficiently close to the true value.

2.3.3. Boundary Conditions. The boundary conditions were chosen to simulate *in vitro* conditions in which a section of fiber mesh is placed over a vaginal multicellular layer. On the edges of the geometry that were theoretically exposed to the inner vaginal cavity, no-flux boundary conditions were assumed:

$$\vec{n}\cdot(D \times \nabla C) = 0 \tag{14a}$$

On the bottom edge of the geometry, corresponding to the end of the stroma region, the solution was held to be zero. On the left and right sides of the geometry, transfer boundary conditions were assumed. If the model domain had been a theoretical tissue cross-section of the vaginal tissue, it would be logical to assume that drug would continue to diffuse laterally along the length of the vaginal tissue:

$$\vec{n}\cdot(D \times \nabla C) = qC \tag{14b}$$

where q is the transfer coefficient out of the region, and is assumed to be equivalent to the lateral diffusion coefficient of tenofovir in the region that contained the boundary.

2.3.4. Initial Conditions. Null concentration was assumed through all regions at time $t = 0$.

2.3.5. Model Parameter Estimation. Previous investigations have observed the release of TFV from PLGA fibers under a range of testing conditions.[7,16] For the degradation model, parameters relating to the kinetics and diffusion of the system were adjusted to produce results matching those of Carson et al.[16] for 100% PLGA fibers containing 15% w/w tenofovir.

For both mathematical models, values of model parameters particular to the delivery vehicle being investigated, namely TFV by means of 50:50 PLGA fibers, were obtained by comparison with other mathematical models[9,11,12,17] or by matching model results to empirical data in the literature.[7,16] By constraining the model to specific empirical data, the results therefrom are considered more relevant in informing design changes and validating the experimental design. The model parameters and their values are summarized in Table 1.

2.3.6. Numerical Implementation. The MATLAB Partial Differential Equation toolbox was used to solve the multicompartmental model. All of the commands were written in a script format; the PDE toolbox user interface was not utilized. The diffusion coefficients, forcing function, and loss rate constants were supplied as nonconstant PDE coefficients in accompanying MATLAB functions. The mesh for the domain consisted of approximately 48 000 triangular elements, and the solution was obtained for the same time period as the degradation model, 30 days.

2.4. Experimental Methods. *2.4.1. Strategy To Obtain Experimental Data.* The data for TFV were obtained from previous work in the literature, which measured the drug release from EFs[16] and calculated the diffusion parameters for a pharmacokinetic compartmental model.[11,12] The drug release of TDF from EFs was measured in our laboratory, as described next.

2.4.2. Electrospun Fiber Synthesis. PLGA polymer (0.55−0.75 dL/g, ∼37−56 kDa, Lactel Absorbable Polymers, Cupertino, CA) was dissolved overnight in 3 mL of 1,1,1,3,3,3-hexafluoro-2-propanol (HFIP, Fisher Scientific, Pittsburgh, PA) to a final concentration of 15% w/w. TDF obtained from crushed Viread tablets (700 mg tablets containing 300 mg TDF, Gilead Sciences Inc., Foster City, CA) was added to the polymer solution to fabricate 1, 10, and 20 wt % drug/wt polymer (w/w) fibers. The presence of inactive excipients in these samples was accounted for when determining the theoretical loading of TDF into polymer fibers. The following day, 2 mL of PLGA-TDF solvent was aspirated into, and electrospun from a 3 mL plastic syringe. All formulations were electrospun with a flow rate of 2.0 mL/h and an applied voltage of 20 kV. EFs were collected on a rotating 4 mm outer-diameter stainless steel mandrel, located 20 cm from the blunt needle tip. Sample flow rate was monitored by an infusion pump (Fisher Scientific, Pittsburgh, PA) and the voltage was applied using a high voltage power supply (Spellman CZE 1000R). After electrospinning, fibers were removed from the mandrel and dried overnight in a desiccator cabinet.

2.4.3. Electrospun Fiber Characterization: Size and Controlled Release. Fiber morphology and diameter were evaluated using scanning electron microscopy (SEM). Desiccated EFs were placed on carbon tape, sputter coated with gold, and imaged using SEM (Supra 35 SEM Zeiss). SEM images were acquired at magnifications ranging from 1000−5000× to enable clear visualization of the fiber microstructure. The average fiber diameter was determined by analyzing SEM images in NIH ImageJ, and drawing line elements across a minimum of 50 fibers per image. Statistical significance between fiber diameters was determined using the Bonferroni post hoc t test ($p < 0.05$).

In vitro release experiments were performed to assess the release of TDF from EFs. Triplicate 10 mg fiber pieces were cut and suspended in 1 mL of simulated vaginal fluid (SVF) to represent intravaginal conditions *in vitro*. SVF was prepared in-house using a previously established protocol.[22] Samples were

DOI: 10.1021/acs.molpharmaceut.7b01089
Mol. Pharmaceutics 2018, 15, 1534−1547

incubated at 37 °C and constantly shaken. The complete volume of SVF was removed and replaced with fresh SVF at time points: 1, 2, 4, 6, 24, 48, 72 h, and 1, 2, 3, and 4 wk. The amount of TDF in the supernatant was measured using HPLC. Quantification was performed using a Viread and TDF standard diluted in SVF, with eluate from blank fibers in SVF used as background correction.

3. RESULTS

3.1. Fiber Characterization. Figure 2 shows representative scanning electron microscopy (SEM) images of the 10% and 20% TDF PLGA fibers. Average fiber diameters were 0.8 ± 0.3 and 1.1 ± 0.4 μm for the 10% and 20% TDF formulations, respectively, demonstrating no statistically significant difference in diameters between formulations. These diameters are consistent with previous 1.0−1.6 μm measurements with 15% TFV PLGA fibers.[16] Total loading of the 10% and 20% TDF fibers was respectively 45.7 ± 0.8 and 82.1 ± 2.5 μg TDF/mg fiber. Both the 10% and 20% TDF formulations demonstrated high encapsulation efficiencies of 81.4 ± 1.5% and 76.3 ± 2.3%, respectively.[18]

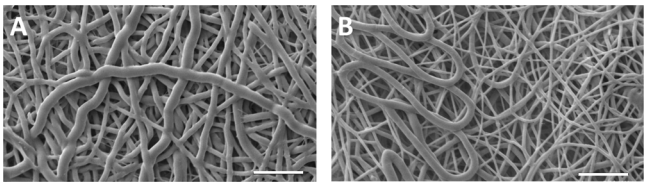

Figure 2. SEM images of PLGA fibers prepared with different drug loading concentrations: (A) 10% and (B) 20% w/w TDF. PLGA fibers were prepared using 15% w/w PLGA in HFIP. Scale bars represent 10 μm.

3.2. Release of TFV. Using the TFV parameters from the literature (as noted in Table 1), the degradation model was used to calculate the release profile of TFV from 15% w/w PLGA fibers, as shown in Figure 3 for both short- (5 d = 120 h) and long-term (30 d = 720 h) release. For fibers with a (default) diameter of 1.0 μm, 15.0% of TFV was released within 24 h (Figure 3A), 40.0% within 240 h, and 65.8% by 720 h (Figure 3B). These results are consistent with the previous *in vitro* studies, which showed 18% and 40% release after 24 h and 240 h, respectively, for 1.0−1.6 μm PLGA fibers with 15% w/w TFV.[16]

Next, the effect of fiber diameter on the drug release was evaluated. In addition to the default 1.0 μm, Figure 3 shows the TFV release profiles from 2.0, and 4.0 μm diameter fibers, resulting in 6.7% and 3.3% of TFV release within 24 h, respectively. For prolonged release spanning 720 h, 36.7% and 19.2% of TFV was released from 2.0 and 4.0 μm fibers, respectively. It should be noted that for these diameter variations, the rate constant of polymer degradation by water, K_d, was changed from 1.9 to 0.1 to fit to our experimental *in vitro* results and to preserve the same parameter values across the three variations.

3.3. Release of TDF. Having established the feasibility of the degradation model using the previously published TFV data, the model was then used with our experimental data to simulate the release of TDF from PLGA fibers of various diameters (Figure 4). To match the modeling results to the significantly higher TDF release rate observed *in vitro*,[16,18] the effective diffusivity of the drug molecules in the polymer matrix was increased by 2 orders of magnitude (1×10^{-17} cm^2/s compared to 3×10^{-15} cm^2/s for TFV and TDF, respectively). For the 1.0 μm fibers, 100% of TDF was released within 24h (Figure 4A,B), while larger diameters of 2.0 and 4.0 μm evinced 84.2% and 50.8% of TDF release within 24h, respectively. During prolonged release, 100% of TDF was released from 2.0 μm fibers by 96 h and by 360 h from 4.0 μm fibers.

The relative concentrations of lactic and glycolic acid in the PLGA formulation, as well as diffusivity differences between TFV and TDF, have been shown to affect the duration and magnitude of the burst release.[23] Previous investigations into this degradation model further showed that the release kinetics were dominated largely by the diffusion of the drug molecules through the polymer matrix;[17] the rate constant governing the mass transfer of drug molecules out of the system had little relative effect. Indeed, when the $k_{C,i}^{ext}$ term for drug was increased or decreased by up to two orders of magnitude, the release profiles were indistinguishable from those resulting from the original value.

In addition to the 15% w/w drug concentration initially used in the model, w/w concentrations of 1%, 5%, 10%, and 20% were also tested. These variations, however, produced no significant change in the drug release profiles. It is likely that drug loading concentrations of 30−40%, as observed in ref 16, are needed to yield increased drug incorporation near the surface, resulting in greater burst release. Further evaluation of the model here showed that the resultant release profile depended almost entirely upon the effective diffusivity of the

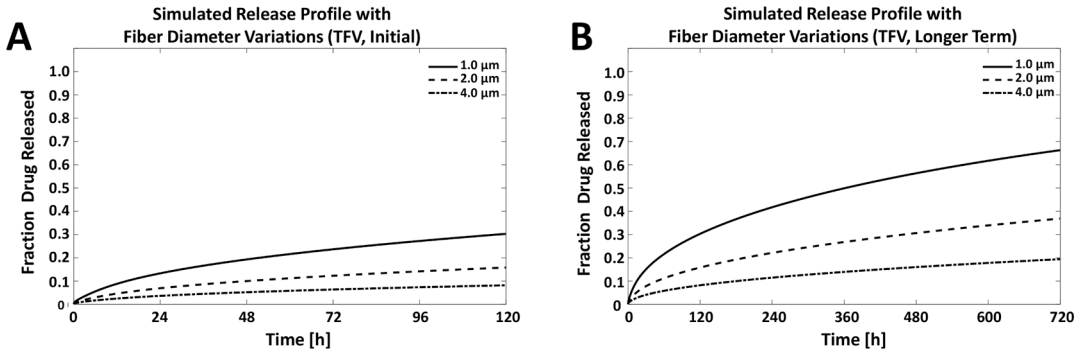

Figure 3. Simulated release profile of TFV from PLGA fibers for (A) 120 h (5 days) and (B) 720 h (30 days). All results are for drug loaded in 100% PLGA fibers with fiber compartment thickness = 0.5 cm. TFV release profiles were simulated with 15% w/w (0.9392 g) loading. PLGA fiber diameter was varied between 1.0, 2.0, and 4.0 μm.

DOI: 10.1021/acs.molpharmaceut.7b01089
Mol. Pharmaceutics 2018, 15, 1534−1547

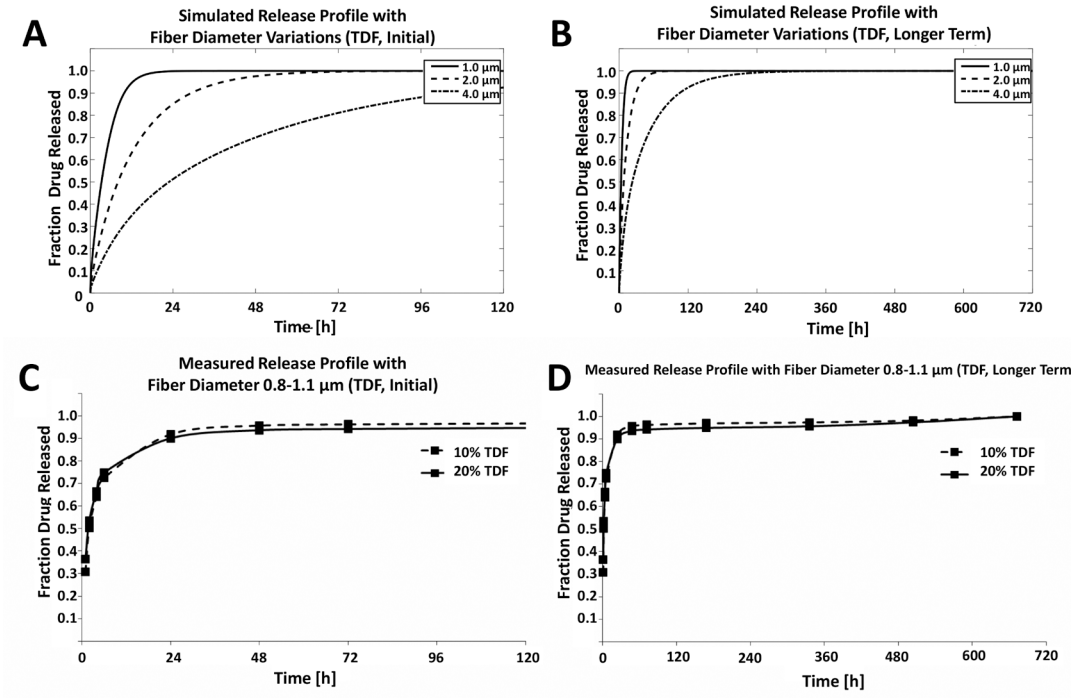

Figure 4. Comparison of TDF release projected by the model to experimental observation. Simulated release profile of TDF from PLGA fibers is shown for (A) 120 h (5 days) and (B) 720 h (30 days). Results are for drug loaded in 100% PLGA fibers with fiber compartment thickness = 0.5 cm. TDF release profiles were simulated with 15% w/w (0.9392g) loading, while fiber diameter was varied between 1.0, 2.0, and 4.0 μm. Experimental observations of *in vitro* release of TDF from PLGA fibers are shown for (C) 120 h (5 days) and (D) 720 h (30 days). The *in vitro* release is based on PLGA EFs loaded with 10 and 20% w/w TDF with diameters 0.8−1.1 μm.

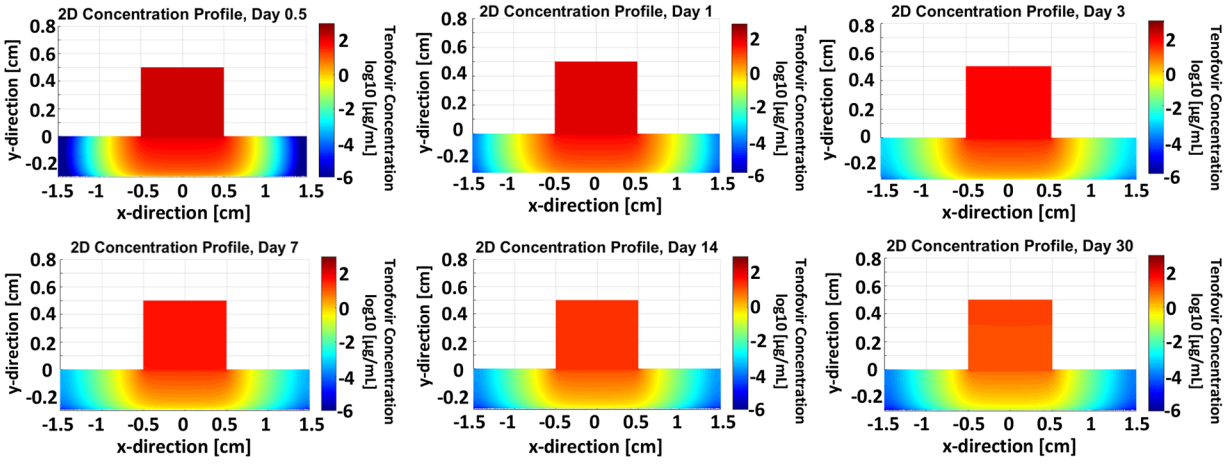

Figure 5. Simulated spatiotemporal distribution of TFV concentration profiles in surrounding fluid, epithelium and stroma (0.5 to 30 d). Results are from 15% w/w TFV incorporated in 100% PLGA fibers of diameter = 1.0 μm, fiber compartment thickness = 0.5 cm.

drug molecules through the polymer matrix, the diameter of the fiber, and the rate constant for the degradation of polymer chains; adjustments in other system variables produced no noticeable change in drug release.

Lastly, the release of TDF projected by the degradation model was compared with *in vitro* release measured experimentally from PLGA EFs incorporating TDF (Figure 4C,D). PLGA EFs encapsulating 10 and 20% TDF were incubated in simulated vaginal fluid for a period up to 4 weeks. The diameter of the fibers ranged from 0.8 to 1.1 μm and yielded 90% release within 24 h, which fell between the 100% and 85% release projected by the simulation for the 1.0 and 2.0 μm diameter fibers, respectively.

3.4. Spatiotemporal Distribution of TFV. Next, the results of the fiber degradation model were fed into the multicompartmental model to evaluate the 2D spatiotemporal distribution of TFV in vaginal tissue (Figures 5−9), for which PK values were available in the literature,[11,12] as well as the compartment-averaged TFV concentration with respect to time (Figure 10). The 2D spatiotemporal distribution is useful in estimating the localization of TFV molecules within the vaginal environment, and the compartment-averaged concentration helps to relate these results to clinically effective TFV concentrations within the vaginal tract for a given duration.

The simulated release profiles of TFV were evaluated from 15% w/w TFV PLGA fibers within the vaginal fluid, epithelium and stroma at various times (12 h through 720 h), for varying

DOI: 10.1021/acs.molpharmaceut.7b01089
Mol. Pharmaceutics 2018, 15, 1534−1547

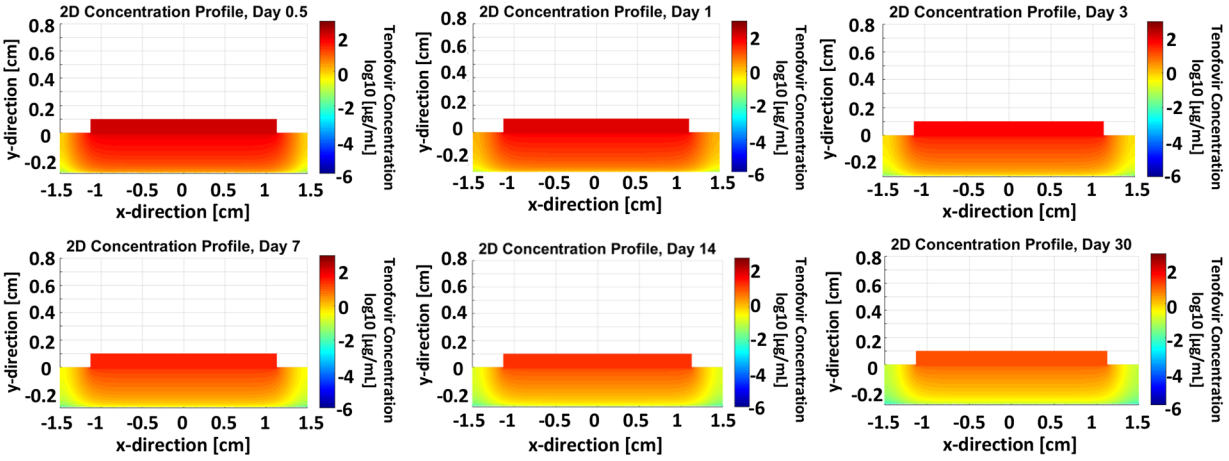

Figure 6. Simulated spatiotemporal distribution of TFV concentration profiles in surrounding fluid, epithelium and stroma (0.5 to 30 d). The fiber compartment thickness was chosen as 0.1 cm, and the radius was recalculated to preserve a fiber volume of 0.4 cm^3. Results had the same release conditions as the degradation model (0.9392 g TFV released from fibers at a 15% w/w concentration).

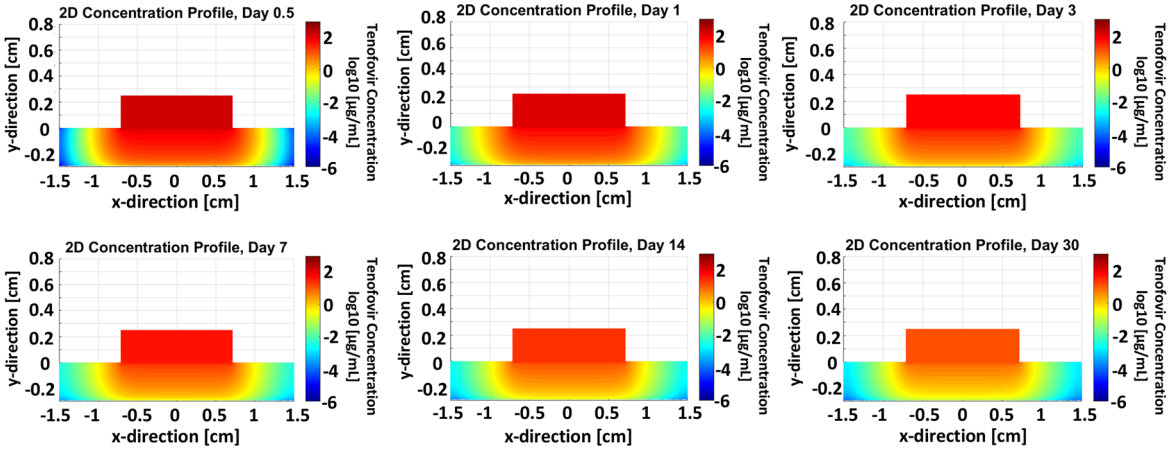

Figure 7. Simulated spatiotemporal distributions of TFV concentration profiles in surrounding fluid, epithelium and stroma (0.5 to 30 d). The fiber compartment thickness was chosen as 0.25 cm, and the radius was recalculated to preserve a fiber volume of 0.4 cm^3. Results had the same release conditions as the degradation model (0.9392 g TFV released from fibers at a 15% w/w concentration).

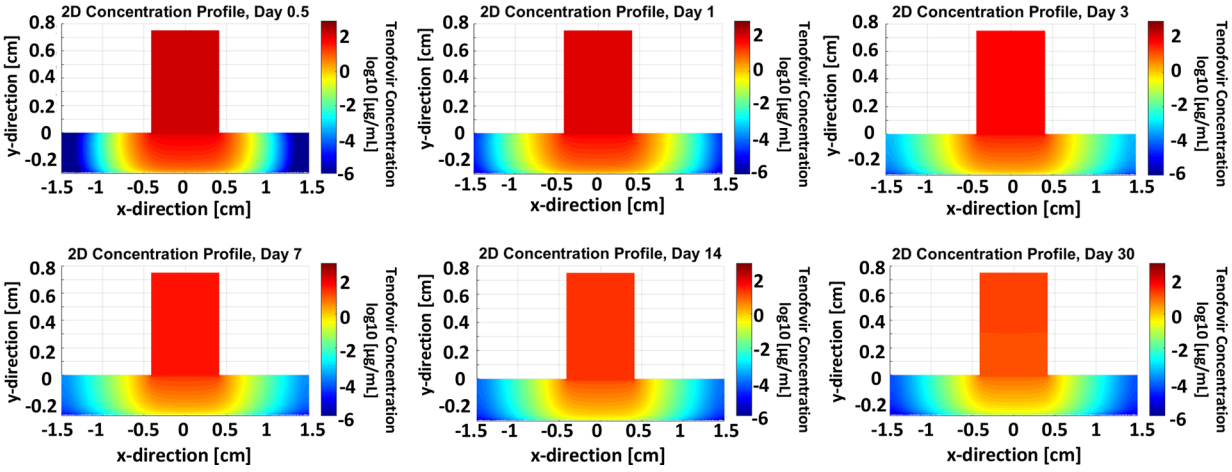

Figure 8. Simulated spatiotemporal distributions of TFV concentration profiles in surrounding fluid, epithelium and stroma (0.5 to 30 d). The fiber compartment thickness was chosen as 0.75 cm, and the radius was recalculated to preserve a fiber volume of 0.4 cm^3. Results had the same release conditions as the degradation model (0.9392 g TFV released from fibers at a 15% w/w concentration).

fiber diameters and thickness. The diffusion of TFV from PLGA fibers with thicknesses of 0.1, 0.25, and 0.75 cm are shown in Figures 6–8, as compared to a baseline of 0.5 cm (Figure 5). The dimensions of the fiber compartment were adjusted to maintain a constant fiber compartment volume of 0.4 cm^3 for each simulation, as this was approximately the

DOI: 10.1021/acs.molpharmaceut.7b01089
Mol. Pharmaceutics 2018, 15, 1534–1547

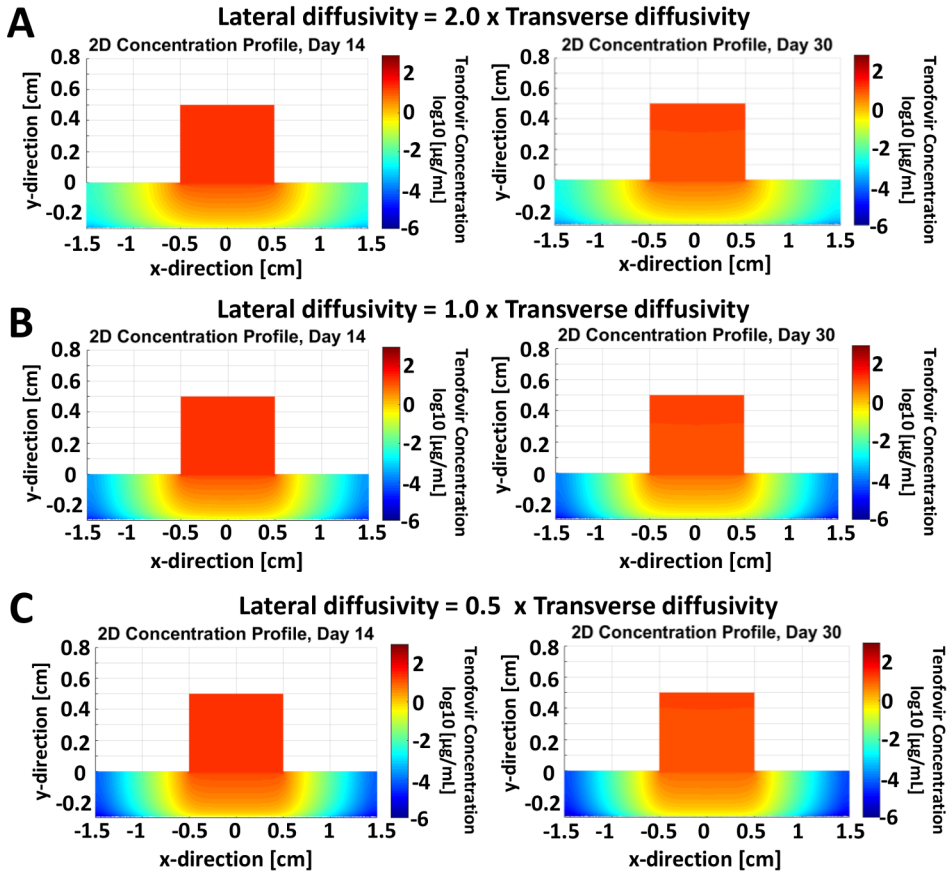

Figure 9. Simulated TFV concentration profiles of fluid, epithelium and stroma with variation in lateral versus traverse diffusivities. The profiles shown for 14 and 30 d include the cases when the lateral diffusivity is (A) twice, (B) equal to, and (C) half that of the transverse diffusion coefficient. All results are from 15% w/w (0.9392g) TFV loaded in 100% PLGA fibers of diameter = 1.0 μm, fiber compartment thickness = 0.5 cm.

volume of the fiber compartment for the radius and thickness dimensions used initially. For future studies, the mass of the fiber mesh could be changed to investigate specific mesh geometries. The thinner fiber meshes (Figure 6) seemed to elicit higher concentrations both on average throughout the tissue and at depths equal to those created by the thicker fibers (Figure 8). It was noted that the aspect ratio for all the concentration profile figures favored the *y*-direction over the x-dimension.

Physical anisotropies in the vaginal canal are expected to affect the diffusion of drug. Adjusting the relative magnitudes of the transverse (*y*-direction) and lateral (*x*-direction) diffusivities produced different pharmacokinetic profiles of TFV at 336 h (14 d) and at 720 h (30 d) postfiber insertion (Figure 9). As expected, the case of lateral diffusivity being twice that of transverse diffusivity evinced better lateral drug diffusion, although with a more superficial profile than the case with lateral diffusivity being half that of transverse diffusivity.

Figure 10 shows the simulated average drug concentration in each compartment over initial (120 h) and longer term (720 h) time for fiber thicknesses of 0.10, 0.25, 0.50, and 0.75 cm. Because of the significant burst release of drug from the release model, the maximum concentration in each of the compartments was achieved within 6 h. Overall, thinner fiber meshes provided higher peak values of TFV concentration in the vaginal tissues as well as higher concentrations after 30 days. The thinner fiber meshes achieved higher concentrations relative to the thicker meshes in the epithelium at both their peak (3.3×10^2, 2.3×10^2, 1.7×10^2 and 1.1×10^2 μg/mL respectively) and after 720 h (9.3, 6.5, 4.3, and 3.3 μg/mL, respectively). Although the concentration of TFV in the epithelium was highest for 0.10 cm and lowest for 0.75 cm fiber thicknesses, the concentration in the vaginal fluid remained at similar levels for all values of thickness (reaching 13 μg/mL by 720 h). In contrast, the concentration in the stroma during this time frame decreased as the fiber thickness increased (ranging from 1.8 to 0.7 μg/mL).

4. DISCUSSION

While EF formulations are often iteratively designed and tested to evaluate the effect of different active agents and fabrication parameters, there is a critical need to develop tools that lend information to the appropriate design of the delivery vehicle as well as transport experiments. Moreover, tools that provide the ability to obtain and link information that would normally be gained through extensive *in vitro*, *ex vivo*, and *in vivo* testing would prove beneficial in streamlining and minimizing iterative experimentation. Mathematical modeling provides a means to inform and expedite formulation development by simultaneously incorporating the effects of a variety of electrospinning parameters to lend predictive potential to fiber design. Traditionally, finite difference equations and finite element models have provided reliably rigorous approaches to accurately predict the molecular pharmacokinetics and transport of a variety of active agents from various delivery platforms.[24−29] By applying these tools to EF design, we expect that the pharmacokinetics of EF-incorporated active agents can be tailored to obtain precise release profiles over

DOI: 10.1021/acs.molpharmaceut.7b01089
Mol. Pharmaceutics 2018, 15, 1534−1547

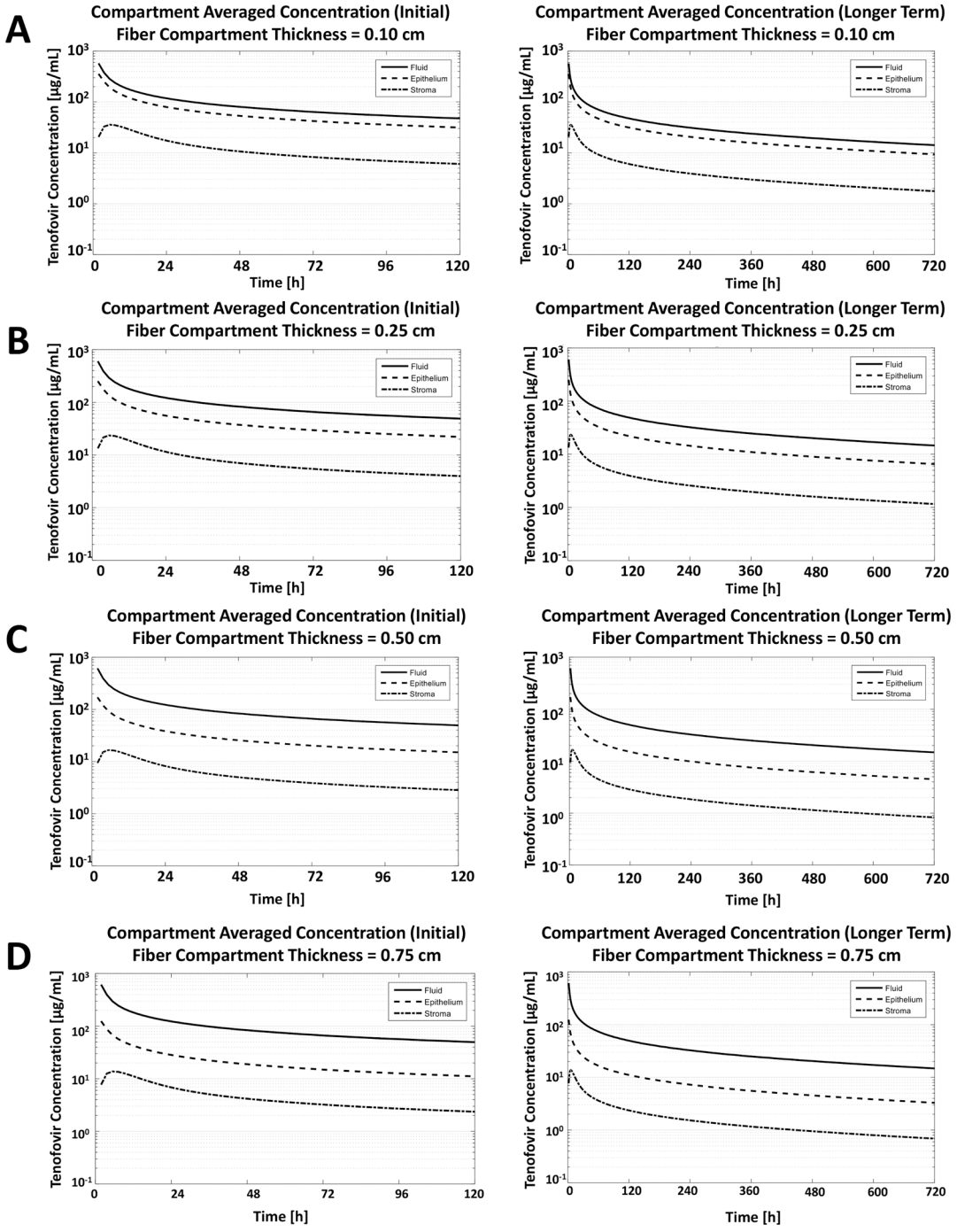

Figure 10. Compartment-averaged TFV concentrations for first 120 h (5 days) and 720 h (30 days). The fiber compartment thickness was varied between: (A) 0.1 cm, (B) 0.25 cm, (C) 0.50 cm (default), and (D) 0.75 cm. All results are from 15% w/w TFV in 100% PLGA fibers of diameter = 1.0 μm.

specific prophylactic or therapeutic durations. Yet, to date, few computational studies have been applied to the design of EF delivery platforms, and to our knowledge, no comparable *in silico* model has been developed that predicts the release of small molecule antiretroviral agents from EFs for application to the FRT. In previous fiber studies for nonreproductive applications, computer modeling was performed either as a supplementary task, to determine the molecular structure and potential surface energy of encapsulants,[30] or to predict the release and distribution of encapsulants into surrounding tissue.[31] Here, we build upon previous modeling that has been applied to different system geometries and kinetics,[11,17] to establish a framework to model the release of antiviral drug from PLGA EFs and localized distribution in the FRT. In particular, we simulate the release of two FDA-approved antiretrovirals, TFV and TDF (a more potent prodrug derivative).

To improve the design of prolonged-release delivery vehicles that satisfy varying design criteria, and to better extrapolate *in vitro* findings to 3D distributions of drugs in tissues, we seek to develop a mathematical framework that can predict the release of given molecules from delivery vehicles (here, electrospun

DOI: 10.1021/acs.molpharmaceut.7b01089
Mol. Pharmaceutics 2018, 15, 1534−1547

fibers) of varying polymers and polymer blends. This study, in which a pair of mathematical models was coupled to predict the release of two structurally similar small molecule antiretrovirals, TFV and TDF, from PLGA EFs, and the spatiotemporal distribution of TFV in the FRT, offers a first step in this direction. Previous *in vitro* experiments have demonstrated significantly different release profiles of these molecules from EFs,[7,16] despite small chemical differences. This study creates a tool to distinguish the release profiles of these two agents within simulated conditions of the vaginal environment, while closely matching the resulting *in silico* data to empirical results obtained *in vitro*. In addition to the immediate ramifications of this effort for the active agents-polymer platform studied here, we expect this work may be expanded to include a diversity of polymers and active agents that have different molecular weights, functional groups, and chemical properties. As an initial analysis, this study requires follow-on work to provide more detailed insight into the variation of system variables. Further, as more sophisticated models are developed, the sink conditions of the degradation model could be replaced with transient concentration levels coupled from the multicompartmental model, and the heterogeneity of the fiber mesh could be included to analyze more granular pharmacodynamics of the drug eluting from this mesh.

While a variety of factors impact the release of active agents from polymeric EFs, perhaps two of the most important are the chemical structure and properties of the active agent. Both TFV and TDF are currently approved as pre-exposure prophylaxis (PrEP) drugs that can be taken daily to prevent HIV-1 infection.[32] While TDF is a slightly larger and more lipophilic prodrug of TFV, both drugs are structurally identical except for the presence in TDF of methyl isopropyl carbonate protecting groups that replace the phosphonic acid hydrogen bond donors of TFV. Yet, despite their structural similarities, recent studies have highlighted the more rapid *in vitro* release of TDF, relative to TFV from PLGA EFs.[16] These data suggest that the phosphonic acid hydrogen bond donors may stabilize or inhibit TFV release from polyester fibers, such as PLGA.[16] Considering the implications of these results to EF design and delivery profiles, we sought to use this information to generate an accurate release model that incorporates the unique diffusivity of structurally similar encapsulants.

The *in silico* results and *in vitro* data obtained from our and others' studies share similar trends, although a few discrepancies were noted. In this study, TFV and TDF release were modeled from PLGA fibers of different diameters, with identical loading concentrations. Irrespective of parameter choice (e.g., drug loading, polymer composition, fiber geometry), *in vitro* studies have shown that TDF releases more rapidly than TFV, particularly from blended polymer fibers.[16] For 1 μm diameter fibers, the model predicts that less than 50% of TFV is released after 240 h (Figure 3), consistent with previous work.[16] In addition, the more gradual release for TFV shown by the *in silico* model during the first 240 h of delivery may be due to the model assumption of polymer chain degradation occurring at the same rate regardless of location within the fiber. Further, our previous *in vitro* studies that show 90% release of TDF within 24 h exposure to aqueous solution[18] validate the release of TDF under similar conditions projected by the mathematical model, for which 100% and 85% release is anticipated for 1.0–2.0 μm diameter fibers within this time frame (Figure 4). For these diameters, complete TDF release from PLGA fibers was achieved after 72 h for both in *in vitro* and *in silico* models, compared to complete release of TDF in 6 h from PCL:PLGA 20:80 composite previously observed.[16]

An important characteristic that affects the release of active agents from EFs is fiber morphology, in particular fiber diameter and thickness.[33−35] As shown in Figure 3, as fiber diameter increases, the rate of encapsulant release decreases. This phenomenon is attributed to the increased surface area-to-volume ratio of smaller diameter fibers, resulting in greater interaction with the surrounding solution. In addition to diameter, fiber mesh thickness also plays an important role in regulating release from EFs, and generally is inversely correlated to release rate.[36] Previous *in vitro* studies have shown that increased EF thickness can delay release and decrease burst release, but this effect is also impacted by the presence of pores between the fiber and fiber layers.[36] As observed and correlated with the *in silico* work presented here, as the fiber thickness increased from 0.10 to 0.75 cm (and overall width decreased), less active agent distributed to underlying tissue, highlighting the importance of contact area and surface coverage in fiber geometry and design (Figures 5−8). Yet, as the ratio of lateral to transverse diffusivity increased, elevated release rates were obtained from fibers of increased thickness (Figure 9). These results highlight that *in silico* work may be applied during the design stages to better understand how and to extent changes in geometry, fiber diameter, and mesh thickness may have on the release and distribution of encapsulated therapeutics.

In addition to these considerations, the distribution and concentration profile of active agent must be related to an appropriate dosage regimen to provide effective HIV prophylaxis. Here, the compartment-averaged drug concentrations was examined over 5 days (120 h) and 30 days (720 h) to assess how drug distribution changes during short- and long-term delivery regimens. Within 5 days, all fiber mesh geometries maintained TFV concentrations in excess of 2.0 μg/mL in the vaginal tissue stroma; however, only the 0.10 and 0.25 cm geometries maintained a concentration exceeding 1.0 μg/mL for 30 days (Figure 10). For comparison, the EC_{50} of TFV against HIV, determined from *in vitro* and *ex vivo* studies was previously measured as 0.9 μg/mL and 97 μg/mL, respectively.[37] This suggests that fiber mesh geometry is an integral consideration for products that seek long-term (e.g., once-a-month) applications. Depending on the fiber geometry and spatial distribution of drug molecules within, a more frequent dosage regimen might be required.

Another pattern observed is that a significant fraction of drug localizes to areas directly beneath the fiber, in contrast to tissue areas downstream or upstream from the fiber mesh (Figure 5). In combination with Figures 6−8, this demonstrates that the localization of drug molecules to certain regions of the fiber or vaginal tissue could lead to localized effectiveness of administration. Generally, the thinner and wider fiber geometry provided more uniform distribution of drug. Combined with the trend of thinner fiber meshes achieving higher peak and long-term TFV concentrations in vaginal tissues (Figure 8), this suggests that when considering fibers of equal mass, those that cover more of the vaginal epithelium will provide more effective short-term and long-term treatment.

Although mathematical modeling is useful for predicting the effects of particular physical parameters on release kinetics, its potential extends beyond the refinement of release profiles. The consideration of fiber geometry and physical properties is additionally important to establish drug pharmacokinetics, and

DOI: 10.1021/acs.molpharmaceut.7b01089
Mol. Pharmaceutics 2018, 15, 1534−1547

for product development considerations that involve early design stage questions, such as user acceptance and preference. In particular, it has been shown that user acceptance is critical to adherence, and hence efficacy, even for well-established technologies such as vaginal rings and films. Previous studies have surveyed user preference of vaginal films that may have similar structural characteristics and administration methods to fibers.[38] In these studies, it was shown that specific macroproperties of films such as size, texture, and level of transparency significantly impacted the user preference and likelihood of use.[38] As an initial step toward modeling product shape and structure, here we sought to relate changes in fiber geometry, by varying fiber thickness and width, while maintaining a constant mass and volume, to estimate drug concentration in the epithelium and stroma. Given a particular configuration or design, these relationships provide an indicator of the effectiveness of the fibers to deliver a threshold concentration of active agent. While simulated alterations in fiber geometry were evaluated to assess changes in the spatiotemporal distribution of released EF encapsulants (Figures 5−9), such modeling also has the potential to integrate this information on user preference with a product design that will be more convenient (and hence effective) in practice. This would enable the prediction of fiber parameters that can provide effective release properties for a given polymer, while informing product geometry/dosage with knowledge important to users.

Another consideration that will increase the utility and applicability of *in silico* studies is accounting for polymer type, composition, and polymer blends.[39−42] These factors introduce another layer of complexity to fiber design and fabrication, impacting both release and loading properties. The concentrations of various polymer species have been used as a means to tailor the release profile of fiber meshes for a particular duration.[7,16] These systems exhibit various regions of zero-order release and burst release, and the modeling of these systems would require system domains that contain granular regions of PLGA and other polymer species. Relating these to fabrication challenges, blended polymers may limit solvent choice, and dramatically affect fabrication parameters including the viscosity, flow rate, and voltage needed for electrospinning. Compounding these considerations is that many of these polymers (e.g., PLGA) are composed of different monomer ratios. By altering the ratio of monomers, properties such as hydrophobicity, rate of degradation, and encapsulation efficiency will change. Finally, the molecular weight of a polymer (or polymers) will affect release rates, with increasing weight conferring decreased rates of fiber degradation. Future mathematical modeling may incorporate the complexities of these relationships between the solvent, polymer blends, as well as chosen encapsulant to guide the design, and minimize fabrication time and iterative benchtop testing of new fiber formulations.

AUTHOR INFORMATION

Corresponding Author

*E-mail: hbfrie01@louisville.edu. Phone: 502-852-3302. Fax: 502-852-6806.

ORCID

Hermann B. Frieboes: 0000-0001-5959-4286

Author Contributions

‖Joint senior authorship. M.E.H. implemented the mathematical models and drafted the initial manuscript. K.M.T. performed the experiments. J.M.S.-R. conceived the study, participated in its design and coordination, and drafted the manuscript. H.B.F. conceived of the study, participated in its design and coordination, and drafted the manuscript. All authors read and approved the final manuscript.

Notes

The authors declare no competing financial interest.

ACKNOWLEDGMENTS

J.M.S.-R. acknowledges partial support from the Jewish Heritage Fund for Excellence. The authors are grateful to Harrison Simrall at the University of Louisville for computing assistance.

REFERENCES

(1) Aniagyei, S. E.; Sims, L. B.; Malik, D. A.; Tyo, K. M.; Curry, K. C.; Kim, W.; Hodge, D. A.; Duan, J.; Steinbach-Rankins, J. M. Evaluation of poly(lactic-co-glycolic acid) and poly(dl-lactide-co-epsilon-caprolactone) electrospun fibers for the treatment of HSV-2 infection. *Mater. Sci. Eng., C* **2017**, *72*, 238−251.

(2) Blakney, A. K.; Ball, C.; Krogstad, E. A.; Woodrow, K. A. Electrospun fibers for vaginal anti-HIV drug delivery. *Antiviral Res.* **2013**, *100* (Suppl), S9−16.

(3) Huang, C.; Soenen, S. J.; van Gulck, E.; Vanham, G.; Rejman, J.; Van Calenbergh, S.; Vervaet, C.; Coenye, T.; Verstraelen, H.; Temmerman, M.; Demeester, J.; De Smedt, S. C. Electrospun cellulose acetate phthalate fibers for semen induced anti-HIV vaginal drug delivery. *Biomaterials* **2012**, *33* (3), 962−9.

(4) Ball, C.; Woodrow, K. A. Electrospun solid dispersions of Maraviroc for rapid intravaginal preexposure prophylaxis of HIV. *Antimicrob. Agents Chemother.* **2014**, *58* (8), 4855−65.

(5) Krogstad, E. A.; Ramanathan, R.; Nhan, C.; Kraft, J. C.; Blakney, A. K.; Cao, S.; Ho, R. J. Y.; Woodrow, K. A. Nanoparticle-releasing nanofiber composites for enhanced in vivo vaginal retention. *Biomaterials* **2017**, *144*, 1−16.

(6) Zong, S.; Wang, X.; Yang, Y.; Wu, W.; Li, H.; Ma, Y.; Lin, W.; Sun, T.; Huang, Y.; Xie, Z.; Yue, Y.; Liu, S.; Jing, X. The use of cisplatin-loaded mucoadhesive nanofibers for local chemotherapy of cervical cancers in mice. *Eur. J. Pharm. Biopharm.* **2015**, *93*, 127−35.

(7) Chou, S.-F.; Woodrow, K. A. Relationships between mechanical properties and drug release from electrospun fibers of PCL and PLGA blends. *Journal of the Mechanical Behavior of Biomedical Materials* **2017**, *65*, 724−733.

(8) Moussy, Y.; Guegan, E.; Davis, T.; Koob, T. J. Transport Characteristics of a Novel Local Drug Delivery System Using Nordihydroguaiaretic Acid (NDGA)-Polymerized Collagen Fibers. *Biotechnol. Prog.* **2007**, *23* (4), 990−994.

(9) Nakielski, P.; Kowalczyk, T.; Kowalewski, T. A. *Modeling drug release from materials based on electrospun nanofibers*; COMSOL Conference, 2013; pp 23−25.

(10) Zeng, L.; An, L.; Wu, X. Modeling drug-carrier interaction in the drug release from nanocarriers. *J. Drug Delivery* **2011**, *2011*, 370308.

(11) Gao, Y.; Katz, D. F. Multicompartmental pharmacokinetic model of tenofovir delivery by a vaginal gel. *PLoS One* **2013**, *8* (9), e74404.

(12) Gao, Y.; Yuan, A.; Chuchuen, O.; Ham, A.; Yang, K. H.; Katz, D. F. Vaginal deployment and tenofovir delivery by microbicide gels. *Drug Delivery Transl. Res.* **2015**, *5* (3), 279−94.

(13) Cu, Y.; Saltzman, W. M. Mathematical modeling of molecular diffusion through mucus. *Adv. Drug Delivery Rev.* **2009**, *61* (2), 101−114.

(14) Grooms, T. N.; Vuong, H. R.; Tyo, K. M.; Malik, D. A.; Sims, L. B.; Whittington, C. P.; Palmer, K. E.; Matoba, N.; Steinbach-Rankins, J. M. Griffithsin-Modified Electrospun Fibers as a Delivery Scaffold To

DOI: 10.1021/acs.molpharmaceut.7b01089
Mol. Pharmaceutics 2018, 15, 1534−1547

Prevent HIV Infection. *Antimicrob. Agents Chemother.* **2016**, *60* (11), 6518−6531.
(15) Steinbach, J. M.; Weller, C. E.; Booth, C. J.; Saltzman, W. M. Polymer nanoparticles encapsulating siRNA for treatment of HSV-2 genital infection. *J. Controlled Release* **2012**, *162* (1), 102−10.
(16) Carson, D.; Jiang, Y.; Woodrow, K. A. Tunable release of multiclass anti-HIV drugs that are water-soluble and loaded at high drug content in polyester blended electrospun fibers. *Pharm. Res.* **2016**, *33* (1), 125−136.
(17) Casalini, T.; Rossi, F.; Lazzari, S.; Perale, G.; Masi, M. Mathematical modeling of PLGA microparticles: from polymer degradation to drug release. *Mol. Pharmaceutics* **2014**, *11* (11), 4036−48.
(18) Tyo, K. M.; Vuong, H. R.; Malik, D. A.; Sims, L. B.; Alatassi, H.; Duan, J.; Watson, W. H.; Steinbach-Rankins, J. M. Multipurpose tenofovir disoproxil fumarate electrospun fibers for the prevention of HIV-1 and HSV-2 infections in vitro. *Int. J. Pharm.* **2017**, *531* (1), 118−133.
(19) Hines, D. J.; Kaplan, D. L. Poly(lactic-co-glycolic) acid-controlled-release systems: experimental and modeling insights. *Crit. Rev. Ther. Drug Carrier Syst.* **2013**, *30* (3), 257−76.
(20) Subramanian, R. S. *Convective Mass Transfer*; Clarkson University, 2014.
(21) Shampine, L. F.; Reichelt, M. W. The MATLAB ODE Suite. *SIAM Journal on Scientific Computing* **1997**, *18*, 1−22.
(22) Owen, D. H.; Katz, D. F. A vaginal fluid simulant. *Contraception* **1999**, *59* (2), 91−5.
(23) Yan, N.; Zhang, X.; Cai, Q.; Yang, X.; Zhou, X.; Wang, B.; Deng, X. The effects of lactidyl/glycolidyl ratio and molecular weight of poly(D,L -lactide-co-glycolide) on the tetracycline entrapment and release kinetics of drug-loaded nanofibers. *J. Biomater. Sci., Polym. Ed.* **2012**, *23* (8), 1005−1019.
(24) Kalyanasundaram, S.; Calhoun, V. D.; Leong, K. W. A finite element model for predicting the distribution of drugs delivered intracranially to the brain. *Am. J. Physiol.* **1997**, *273* (5 Pt 2), R1810−21.
(25) Plontke, S. K.; Siedow, N.; Wegener, R.; Zenner, H. P.; Salt, A. N. Cochlear pharmacokinetics with local inner ear drug delivery using a three-dimensional finite-element computer model. *Audiol. Neuro-Otol.* **2007**, *12* (1), 37−48.
(26) Zunino, P. Multidimensional Pharmacokinetic Models Applied to the Design of Drug-Eluting Stents. *Cardiovascular Engineering: An International Journal* **2004**, *4* (2), 181−191.
(27) Wang, Z.; Keith Nelson, J.; Hillborg, H.; Zhao, S.; Schadler, L. S. Dielectric constant and breakdown strength of polymer composites with high aspect ratio fillers studied by finite element models. *Compos. Sci. Technol.* **2013**, *76*, 29−36.
(28) Geonnotti, A. R.; Katz, D. F. Compartmental transport model of microbicide delivery by an intravaginal ring. *J. Pharm. Sci.* **2010**, *99* (8), 3514−21.
(29) Zhang, J.; Zhao, X.; Suo, Z.; Jiang, H. A finite element method for transient analysis of concurrent large deformation and mass transport in gels. *J. Appl. Phys.* **2009**, *105* (9), 093522.
(30) Shaikh, R. P.; Kumar, P.; Choonara, Y. E.; du Toit, L. C.; Pillay, V. Crosslinked electrospun PVA nanofibrous membranes: elucidation of their physicochemical, physicomechanical and molecular disposition. *Biofabrication* **2012**, *4* (2), 025002.
(31) Szabo, P.; Daroczi, T. B.; Toth, G.; Zelko, R. In vitro and in silico investigation of electrospun terbinafine hydrochloride-loaded buccal nanofibrous sheets. *J. Pharm. Biomed. Anal.* **2016**, *131*, 156−159.
(32) Nicol, M. R.; Adams, J. L.; Kashuba, A. D. HIV PrEP Trials: The Road to Success. *Clin. Invest. (London, U. K.)* **2013**, *3* (3), 295.
(33) Sill, T. J.; von Recum, H. A. Electrospinning: applications in drug delivery and tissue engineering. *Biomaterials* **2008**, *29* (13), 1989−2006.
(34) Hu, X.; Liu, S.; Zhou, G.; Huang, Y.; Xie, Z.; Jing, X. Electrospinning of polymeric nanofibers for drug delivery applications. *J. Controlled Release* **2014**, *185*, 12−21.
(35) Kim, G.; Yoon, H.; Park, Y. Drug release from various thicknesses of layered mats consisting of electrospun polycaprolactone and polyethylene oxide micro/nanofibers. *Appl. Phys. A: Mater. Sci. Process.* **2010**, *100* (4), 1197−1204.
(36) Han, N.; Bradley, P. A.; Johnson, J.; Parikh, K. S.; Hissong, A.; Calhoun, M. A.; Lannutti, J. J.; Winter, J. O. Effects of hydrophobicity and mat thickness on release from hydrogel-electrospun fiber mat composites. *J. Biomater. Sci., Polym. Ed.* **2013**, *24* (17), 2018−30.
(37) Nicol, M. R.; Emerson, C. W.; Prince, H. M. A.; Nelson, J. A. E.; Fedoriw, Y.; Sykes, C.; Geller, E. J.; Patterson, K. B.; Cohen, M. S.; Kashuba, A. D. M. Models for Predicting Effective HIV Chemoprevention in Women. *JAIDS, J. Acquired Immune Defic. Syndr.* **2015**, *68* (4), 369−376.
(38) Fan, M. D.; Kramzer, L. F.; Hillier, S. L.; Chang, J. C.; Meyn, L. A.; Rohan, L. C. Preferred Physical Characteristics of Vaginal Film Microbicides for HIV Prevention in Pittsburgh Women. *Arch. Sex. Behav.* **2017**, *46* (4), 1111−1119.
(39) Pillay, V.; Dott, C.; Choonara, Y. E.; Tyagi, C.; Tomar, L.; Kumar, P.; du Toit, L. C.; Ndesendo, V. M. K. A Review of the Effect of Processing Variables on the Fabrication of Electrospun Nanofibers for Drug Delivery Applications. *J. Nanomater.* **2013**, *2013*, 22.
(40) Huang, Z.-M.; Zhang, Y. Z.; Kotaki, M.; Ramakrishna, S. A review on polymer nanofibers by electrospinning and their applications in nanocomposites. *Compos. Sci. Technol.* **2003**, *63* (15), 2223−2253.
(41) Gunatillake, P. A.; Adhikari, R. Biodegradable synthetic polymers for tissue engineering. *European cells & materials* **2003**, *5*, 1−16.
(42) Caballero-George, C.; Marin, E.; Briceno, M. I. Critical evaluation of biodegradable polymers used in nanodrugs. *Int. J. Nanomed.* **2013**, *8*, 3071−90.

DOI: 10.1021/acs.molpharmaceut.7b01089
Mol. Pharmaceutics 2018, 15, 1534−1547